# A New STATCOM Model for Power Flows Using the Newton-Raphson Method

Enrique Acha, *Senior Member, IEEE,* and Behzad Kazemtabrizi, *Member, IEEE*

***Abstract* — The paper presents a new model of the STATCOM aimed at power flow solutions using the Newton-Raphson method. The STATCOM is made up of the series connection of a Voltage Source Converter (VSC) and its connecting transformer. The VSC is represented in this paper by a complex tap-changing transformer whose primary and secondary windings correspond, notionally speaking, to the VSC's AC and DC buses, respectively. The magnitude and phase angle of the complex tap changer are said to be the amplitude modulation index and the phase shift that would exist in a PWM inverter to enable either reactive power generation or absorption purely by electronic processing of the voltage and current waveforms within the VSC. The new STATCOM model allows for a comprehensive representation of its AC and DC circuits – this is in contrast to current practice where the STATCOM is represented by an equivalent variable voltage source, which is not amenable to a proper representation of the STATCOM's DC circuit. One key characteristic of the new VSC model is that no special provisions within a conventional AC power flow solution algorithm is required to represent the DC circuit, since the complex tap-changing transformer of the VSC gives rise to the customary AC circuit and a notional DC circuit. The latter includes the DC capacitor, which in steady-state draws no current, and a current-dependent conductance to represent switching losses. The ensuing STATCOM model possesses unparalleled control capabilities in the operational parameters of both the AC and DC sides of the converter. The prowess of the new STATCOM power flow model is demonstrated by numerical examples where the quadratic convergence characteristics of the Newton-Raphson method are preserved.**

***Index Terms* — FACTS, STATCOM, Voltage Source Converter (VSC), Newton-Raphson method, power flows**

## I. INTRODUCTION

THE STATCOM is a key element of the FACTS technology. It is the modern counterpart of the well-established Static Var Compensator (SVC) and forms the basic building block with which other more advanced FACTS equipment may be built, such as the UPFC and the various forms of VSC-HVDC links. Indeed, the latter application has blurred the line between the FACTS and HVDC transmission options. In its most basic form, the STATCOM may be seen to comprise a voltage source converter (VSC) and a connecting transformer which, more often than not, is a load tap-changing (LTC) transformer [1]-[2]. Current models aimed at fundamental frequency studies have it represented as a controllable voltage source behind a coupling impedance, very much in the same vein as the model of a synchronous condenser [2]-[3]. This simple concept represents well the fact that at the fundamental frequency, the STATCOM converter's output voltage may be adjusted against the AC system's voltage to achieve very tight control targets, a capability afforded by the switched-mode converter technology [1]-[8]. By way of example, the reactive power flow may be controlled by adjusting the converter's output voltage magnitude against the AC system voltage [1]-[2]. The controllable voltage source concept explains the STATCOM's steady-state operation from the vantage of its AC side. However, it fails to explain its operation from the DC side. A notable exception is the equivalent voltage source model reported in [9], where the STATCOM's AC voltage is expressed as a function of the DC voltage and the amplitude modulation ratio. Nevertheless, incorporation of the switching losses in the DC bus or a DC load would be difficult to represent in this model owing to its equivalent voltage source nature. In most STATCOM models aimed at fundamental frequency power flows there is no easy way to ascertaining whether or not the converter's operation is within the linear region of operation [10]. Also, the switching losses tend to be neglected, and the ohmic losses of the converter, along with the effects of the converter's magnetics, are normally lumped together with those of the interfacing transformer.

To circumvent these shortcomings, a new STATCOM model is put forward in this paper where the VSC is represented by a notional tap-changing transformer and a variable shunt susceptance. The primary and secondary sides of this tap-changing transformer may be interpreted as the VSC's AC and DC sides, respectively. Such a VSC model takes into account, in an aggregated form, the phase shifting and scaling nature of the PWM control. That is, its magnitude and phase angle are assigned to be the amplitude modulation index and the phase shift that would exist in a PWM inverter to enable either reactive power generation or absorption purely by electronic processing of the voltage and current waveforms within the VSC. It should be noted that the VSC is designed to operate on a constant DC voltage and that a relatively small capacitor is used to support and stabilize the voltage at its DC bus. Moreover, this small rating capacitor does not contribute *per se* to the reactive

Enrique Acha is with the Department of Electrical Energy Engineering at the Tampere University of Technology (TUT), Tampere, Finland. (email: enrique.acha@tut.fi). Behzad Kazemtabrizi is with the School of Engineering and Computer Science of the University of Durham, Durham, England, UK (e-mail: behzad.kazemtabrizi@durham.ac.uk ).

power exchange with the power grid [11]. The new model takes due account of the VSC switching and ohmic losses separately. It should be noted that in the new VSC model no special provisions within a conventional AC power flow solution algorithm is required to represent the DC circuit. The reason is that the complex tap-changing transformer of the VSC yields the customary AC circuit and a notional DC circuit. The VSC model is series-connected with the LTC transformer model to make up the new STATCOM representation; a model with enhanced control capabilities in the operational parameters of both the AC and DC sides of the converter. Such control modelling flexibility attains special relevance when applied to the realm of VSC-HVDC or UPFC but these subject matters are topics of forthcoming publications. It should be pointed out that the concept of a complex ideal transformer to model a VSC has been applied elsewhere in connection with the UPFC [12, 13]. However, its shunt-connected VSC is represented by a variable susceptance and it is only its series-connected VSC that is represented by a complex ideal transformer –such an approach represents only an approximation to the conventional two-voltage source model of the UPFC [14, 15]. More importantly, both UPFC models, that reported in [12, 13] and that reported in [14, 15], lack DC bus representation.

## II. New VSC Model

### A. VSC main characteristics

The STATCOM comprises the series connection of a VSC and an LTC transformer whose primary winding is shunt-connected with the AC power network. Physically, the VSC is built as a two-level or a multi-level inverter that uses a converter bridge made up of self-commutating switches driven by PWM control. It uses a small capacitor bank on its DC side to support and stabilize the DC voltage to enable converter operation. The converter keeps the capacitor charged to the required voltage level by making its output voltage lag the AC system voltage by a small phase angle [1]. The DC capacitor bank of value $C_{DC}$ is shown schematically in Fig. 1(a). It should be stated that $C_{DC}$ is not used *per se* in the VAR generation/absorption process. Instead, this process is carried out by action of the PWM control which shifts the voltage and current waveforms within the VSC to yield either leading or lagging VAR operation to satisfy operational requirements.

It is said that the VSC has no inertia, its response is practically instantaneous, it does not significantly alter the existing system impedance and it can internally generate reactive (both capacitive and inductive) power [11]. For the purpose of fundamental frequency analysis, the VSC's electronic processing of the voltage and current waveforms is well synthesized by the notional variable susceptance, $B_{eq}$, which connects to the AC bus of the ideal complex tap-changing transformer - see Fig. 1(b). Note that $B_{eq}$ is responsible for the whole of the reactive power production in the valve set of the VSC.

### B. VSC nodal admittance matrix representation

The fundamental frequency operation of the VSC shown schematically in Fig. 1(a) may be modeled by means of electric circuit components, as shown in Fig. 1(b). From the conceptual point of view, the central component of this VSC model is the ideal tap-changing transformer with complex tap which, in the absence of switching losses, may be seen to act as a *nullator* that constrains the source current to zero, with the source being the capacitor $C_{DC}$, and the associated *norator* being the variable susceptance $B_{eq}$ [17]. Indeed, in steady-state operation the DC capacitor may be represented as a battery that yields voltage $E_{DC}$ and draws no current [18] – this point is addressed in more detail in Appendix A. Notice that the winding connected to node 1 is an AC node internal to the VSC and that the winding connected to node 0 is a notional DC node. Two elements connect to the VSC's DC bus, namely, the source, $E_{DC}$, and the current–dependent resistor, $G_{sw}$. Hence, the ideal tap-changing transformer is the element that provides the interface for the VSC's AC and DC circuits, as illustrated in Fig. 1(b). It should be emphasized that no reactive power flows through it, only *real* power which is akin to DC power.

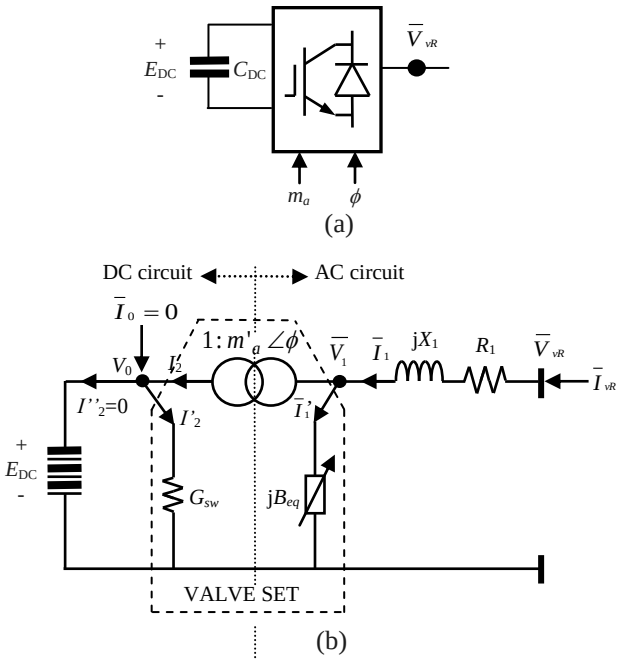


Figure 1: (a) VSC Schematic Representation; (b) VSC equivalent circuit

We have drawn our inspiration to develop this model, from the following basic relationship:

$$\bar{V}_1 = m'_a \, e^{j\phi} E_{DC} \tag{1}$$

where the tap magnitude $m'_a$ of the ideal tap-changing transformer corresponds to the VSC's amplitude modulation coefficient where the following relationship holds for a two-level, three-phase VSC: $m'_a = \sqrt{3}/2 \cdot m_a$, where in the linear range of modulation, the amplitude modulation index $m_a$ takes values within bounds: $0 < m_a < 1$ [19]. The phase

angle $\phi$ is the phase angle of the complex voltage $\bar{V}_1$ relative to the system phase reference, and $E_{\rm DC}$ is the DC bus voltage which is a real scalar and on a per-unit basis carries a value of $\sqrt{2}$.

Other elements of the electric circuit shown in Fig. 1(b) are the series impedance which is connected to the ideal transformer's AC side. The series reactance $X_1$ represents the VSC's interface magnetics. The series resistor $R_1$ accounts for the ohmic losses which are proportional to the AC terminal current squared. Note that the secondary winding current $I_2$ which is always a real quantity, splits into $I'_2$ and $I''_2$. The latter current is always zero during steady-state operation. This is further elaborated in Appendix A, where the role of the VSC's phase-shifting transformer is analyzed from the vantage of electronic circuits [17].

As one would expect, the complex power conservation property of the ideal transformer in Fig. 1(b) stands but note that there is no reactive power flowing through it, since all the reactive power requirements of the VSC model (generation/absorption) are met by the shunt branch $B_{eq}$ connected at node 1. The power relationships between nodes 1 and 0, which account for the full VSC model, are:

$$V_0 I_2 = \bar{V}_1(\bar{I}_1^* - \bar{I}_1^*) = \bar{V}_1\bar{I}_1^* + \mathrm{j}B_{eq}V_1^2 \;\Rightarrow\; V_0 I_2 = \mathrm{Re}\left\{\bar{V}_1\bar{I}_1^*\right\} \tag{2}$$

The switching loss model corresponds to a constant resistance (conductance) $G_0$, which under the presence of constant DC voltage and constant load current, would yield constant power loss for a given switching frequency of the PWM converter. Admittedly, the constant resistance characteristic may be inaccurate because although the DC voltage is kept largely constant, the load current will vary according to the prevailing operating condition. Hence, it is proposed that the resistance characteristic derived at rated voltage and current be corrected by the quadratic ratio of the actual current to the nominal current,

$$G_0 \cdot \left(\frac{I_2^{\rm act}}{I_2^{\rm nom}}\right)^2 \;\Rightarrow\; G_{sw} \tag{3}$$

where $G_{\rm sw}$ would be a resistive term exhibiting a degree of power behavior.

The voltage and current relationships in the ideal tap-changing transformer are:

$$\frac{\bar{V}_1}{V_0} = \frac{m'_a\angle\phi}{1} \quad\text{and}\quad \frac{m'_a\angle-\phi}{1} = \frac{I_2}{\bar{I}_1 - \bar{I}'_1} \tag{4}$$

The current through the admittance connected between nodes *vR* and 1 is:

$$\bar{I}_1 = \bar{Y}_1\left(\bar{V}_{vR} - \bar{V}_1\right) = \bar{Y}_1\bar{V}_{vR} - m'_a\angle\phi\,\bar{Y}_1 V_0 = \bar{I}_{vR} \tag{5}$$

where $\bar{Y}_1 = 1/(R_1 + \mathrm{j}X_1)$.

At node 0, the following relationship holds:

$$\begin{aligned}\bar{I}_0 &= -I_2 + I'_2 = -m'_a\angle-\phi(\bar{I}_1 - \bar{I}'_1) + G_{sw}V_0 \\ &= -m'_a\angle-\phi\bar{Y}_1\bar{V}_{vR} + G_{sw}V_0 + m'^2_a\left(\bar{Y}_1 + \mathrm{j}B_{eq}\right)V_0\end{aligned} \tag{6}$$

Combining (5) and (6) and incorporating constraints from the electric circuit in Fig. 1(b):

$$\begin{pmatrix}\bar{I}_{vR}\\ \bar{I}_0 = 0\end{pmatrix} = \begin{pmatrix}\bar{Y}_1 & -m'_a\angle\phi\bar{Y}_1\\ -m'_a\angle-\phi\bar{Y}_1 & G_{sw} + m'^2_a(\bar{Y}_1 + \mathrm{j}B_{eq})\end{pmatrix}\begin{pmatrix}\bar{V}_{vR}\\ V_0 = E_{\rm DC}\end{pmatrix} \tag{7}$$

and more explicitly:

$$\begin{pmatrix}\bar{I}_{vR}\\ \bar{I}_0 = 0\end{pmatrix} = \begin{pmatrix}\bar{Y}_1 & -m'_a(\cos\phi + \mathrm{j}\sin\phi)\bar{Y}_1\\ -m'_a(\cos\phi - \mathrm{j}\sin\phi)\bar{Y}_1 & G_{sw} + m'^2_a(\bar{Y}_1 + \mathrm{j}B_{eq})\end{pmatrix}\begin{pmatrix}\bar{V}_{vR}\\ V_0 = E_{\rm DC}\end{pmatrix} \tag{8}$$

Notice that this expression represents the VSC equivalent circuit in Fig. 1(b) in steady-state, with the capacitor effect represented by the DC voltage $E_{\rm DC}$.

### *C. VSC nodal power equations*

The complex power model is derived from the nodal admittance matrix where, subsequently, the DC voltage will be referred only as $V_0$ as opposed to $E_{\rm DC}$:

$$\begin{aligned}\begin{pmatrix}\bar{S}_{vR}\\ \bar{S}_0\end{pmatrix} &= \begin{pmatrix}\bar{V}_{vR} & 0\\ 0 & V_0\end{pmatrix}\begin{pmatrix}\bar{I}^*_{vR}\\ \bar{I}^*_0\end{pmatrix} \\ &= \begin{pmatrix}\bar{V}_{vR} & 0\\ 0 & V_0\end{pmatrix}\left\{\begin{pmatrix}\bar{Y}_1^* & -m'_a(\cos\phi - \mathrm{j}\sin\phi)\bar{Y}_1^*\\ -m'_a(\cos\phi + \mathrm{j}\sin\phi)\bar{Y}_1^* & G_{sw} + m'^2_a(\bar{Y}_1^* - \mathrm{j}B_{eq})\end{pmatrix}\begin{pmatrix}\bar{V}^*_{vR}\\ V_0\end{pmatrix}\right\}\end{aligned} \tag{9}$$

Following some arduous algebra, the nodal active and reactive power expressions are arrived at:

$$\begin{aligned}P_{vR} &= G_1V_{vR}^2 - m'_aV_{vR}V_0\left[G_1\cos(\theta_{vR} - \theta_0 - \phi) + B_1\sin(\theta_{vR} - \theta_0 - \phi)\right]\\ Q_{vR} &= -B_1V_{vR}^2 - m'_aV_{vR}V_0\left[G_1\sin(\theta_{vR} - \theta_0 - \phi) - B_1\cos(\theta_{vR} - \theta_0 - \phi)\right]\\ P_0 &= (m'^2_aG_1 + G_{sw})V_0^2 - m'_aV_{vR}V_0\left[G_1\cos(\theta_0 - \theta_{vR} + \phi) + B_1\sin(\theta_0 - \theta_{vR} + \phi)\right]\\ Q_0 &= -m'^2_a(B_1 + B_{eq})V_0^2 - m'_aV_{vR}V_0\left[G_1\sin(\theta_0 - \theta_{vR} + \phi) - B_1\cos(\theta_0 - \theta_{vR} + \phi)\right]\end{aligned} \tag{10}$$

### *D. VSC linearized system of equations*

These equations are non-linear and their solution, for a pre-defined set of generation and load pattern may be carried out using the Newton-Raphson method. This involves repeated linearization of the nodal power equations. Their initial evaluation requires an informed guess of the state variable values: $(\theta_{vR}^{(0)}, V_{vR}^{(0)}, \theta_0^{(0)}, m'^{(0)}_a, \phi^{(0)}, B_{eq}^{(0)})$, when the aim is to regulate voltage magnitude at bus *vR* using the VSC's amplitude modulation ratio ($m_a'$) and keep $V_0$ at a constant value. In practice, the latter is possible due to the DC capacitor's action. The linearized system of equations is:

$$\begin{bmatrix}\Delta P_{vR}\\ \Delta Q_{vR}\\ \Delta P_0\\ \Delta Q_0\\ \Delta P_{0\text{-}vR}\\ \Delta Q_{0\text{-}vR}\end{bmatrix} = \left[\begin{array}{cc:cc:cc}\partial P_{vR}/\partial\theta_{vR} & (\partial P_{vR}/\partial m'_a)m'_a & \partial P_{vR}/\partial\theta_0 & 0 & \partial P_{vR}/\partial\phi & \partial P_{vR}/\partial B_{eq}\\ \partial Q_{vR}/\partial\theta_{vR} & (\partial Q_{vR}/\partial m'_a)m'_a & \partial Q_{vR}/\partial\theta_0 & 0 & \partial Q_{vR}/\partial\phi & \partial Q_{vR}/\partial B_{eq}\\ \hdashline \partial P_0/\partial\theta_{vR} & (\partial P_0/\partial m'_a)m'_a & \partial P_0/\partial\theta_0 & 0 & \partial P_0/\partial\phi & \partial P_0/\partial B_{eq}\\ 0 & 0 & 0 & 1 & 0 & 0\\ \hdashline \partial P_{0\text{-}vR}/\partial\theta_{vR} & (\partial P_{0\text{-}vR}/\partial m'_a)m'_a & \partial P_{0\text{-}vR}/\partial\theta_0 & 0 & \partial P_{0\text{-}vR}/\partial\phi & \partial P_{0\text{-}vR}/\partial B_{eq}\\ \partial Q_{0\text{-}vR}/\partial\theta_{vR} & (\partial Q_{0\text{-}vR}/\partial m'_a)m'_a & \partial Q_{0\text{-}vR}/\partial\theta_0 & 0 & \partial Q_{0\text{-}vR}/\partial\phi & \partial Q_{0\text{-}vR}/\partial B_{eq}\end{array}\right]\begin{bmatrix}\Delta\theta_{vR}\\ \Delta m'_a/m'_a\\ \Delta\theta_0\\ \Delta V_0/V_0\\ \Delta\phi\\ \Delta B_{eq}\end{bmatrix} \tag{11}$$

Subsequent evaluations of the nodal power equations are

carried out using the improved set of values being furnished by the iterative process: $(\theta_{vR}^{(r)}, V_{vR}^{(r)}, \theta_0^{(r)}, m'^{(r)}_a, \phi^{(r)}, B_{eq}^{(r)})$, where $(r)$ is the iteration counter. In this application, the regulated powers $P_{0-vR,\text{reg}}$ and $Q_{0-vR,\text{reg}}$ also form part of the control set. The entries making up eq. (11) are given in Appendix B.

*1) Mismatch power terms and control variables:*

A mismatch power term is the difference between the net power and the calculated power at a given bus, say *vR*, and 0. The calculated powers are determined using the nodal power equations (10), giving,

$$\begin{aligned}
\Delta P_{vR} &= P_{vR,\text{net}} - P_{vR,\text{cal}} = (P_{vR,\text{gen}} - P_{vR,\text{load}}) - P_{vR,\text{cal}} \\
\Delta Q_{vR} &= Q_{vR,\text{net}} - Q_{vR,\text{cal}} = (Q_{vR,\text{gen}} - Q_{vR,\text{load}}) - Q_{vR,\text{cal}} \\
\Delta P_0 &= P_{0,\text{net}} - P_{0,\text{cal}} = (P_{0,\text{gen}} - P_{0,\text{load}}) - P_{0,\text{cal}} \\
\Delta Q_0 &= Q_{0,\text{net}} - Q_{0,\text{cal}} = (Q_{0,\text{gen}} - Q_{0,\text{load}}) - Q_{0,\text{cal}} \\
\Delta P_{0-vR} &= P_{0-vR,\text{reg}} - P_{0-vR,\text{cal}} \\
\Delta Q_{0-vR} &= Q_{0-vR,\text{reg}} - Q_{0-vR,\text{cal}}
\end{aligned} \tag{12}$$

The mismatch power flow in branch *vR*-0 is the difference between the target power flow at the branch and the calculated power. In the VSC application, both active and reactive power targets are normally set to zero.

*2) State variables and increments:*

The state variable increments calculated at iteration $(r)$ with the power flow model are:

$$\begin{aligned}
\Delta\theta_{vR}^{(r)} &= \theta_{vR}^{(r)} - \theta_{vR}^{(r-1)} \\
\Delta m'^{(r)}_a &= m'^{(r)}_a - m'^{(r-1)}_a \\
\Delta\theta_0^{(r)} &= \theta_0^{(r)} - \theta_0^{(r-1)} \\
\Delta\phi^{(r)} &= \phi^{(r)} - \phi^{(r-1)} \\
\Delta B_{eq}^{(r)} &= B_{eq}^{(r)} - B_{eq}^{(r-1)}
\end{aligned} \tag{13}$$

*3) Non-regulated solutions:*

If no voltage regulation at node *vR* is applied, the voltage magnitude $V_{vR}$ replaces $m'_a$ as state variable in the linearized power flow equation (11). Other control options may be available, but some caution needs to be exercised in the VSC and STATCOM applications because power regulation at node *vR* cannot be achieved since the internal power losses are not known a priori, and voltage control in the DC node 0 is achieved by virtue of the DC capacitor.

*4) Practical implementations:*

*a) Control Strategy:*

As illustrated in Fig. 1(b), the VSC is assumed to be connected between a sending bus, *vR*, and a receiving bus, 0, with the former taken to be the VSC's AC bus and the latter taken to be the VSC's DC bus. The voltage $V_0$ is kept constant by the action of a small DC capacitor bank with rated capacitance $C_{DC}$, which in steady-state draws no current. In the Newton-Raphson power flow solution the DC bus will be treated as a *PV*-type node with zero nodal power injection and a constant voltage magnitude of value $E_{\text{DC}}$. Likewise, the voltage magnitude $|V_{vR}|$ is regulated within system-dependent maximum and minimum values, afforded by the following basic relationship:

$$|V_{vR}| = m'_a \, E_{DC} - \sqrt{R_1^2 + X_1^2} \cdot |\bar{I}_1| \tag{14}$$

Note that in the VSC's linear range of modulation, the index $m_a$ takes values within the bounds: $0 < m_a < 1$ and that $m'_a = \sqrt{3}/2 \cdot m_a$. However, in power systems reactive power control applications, it is unlikely that values of $m_a$ lower than 0.5 will be used. The reason is that voltage magnitude at the VSC's AC bus must be kept within practical limits because too high a voltage may induce insulation coordination failure at the point of connection with the power grid and too low a voltage may induce a condition of voltage collapse. Note that with realistic values of $R_1$=0.001 p.u., $X_1$=0.01 p.u. and $E_{DC}$=√2 p.u. and considering low-current operation, say 0.1 p.u., $|V_{vR}|$ will take a value of 0.6114 p.u. with $m_a$=0.5. In the power flow solution the active and reactive powers are regulated on the VSC's DC bus – the former is set to either zero or to a specified DC load, whereas the latter is always set to zero.

*b) Simplifying assumptions:*

A key feature of this model is that the phase angle value at node 0 is independent of circuit parameters or network complexity to the left of the phase-shifting transformer. The reason is that the ideal phase shifter decouples, angle-wise, the circuits to the left and to the right of the ideal transformer. Moreover, the phase angle voltage at bus 0 keeps its value given at the point of initialization. Hence, in the application pursued in this paper, it makes sense to stick to zero phase angle voltage initialization for this bus - when looked at it from the vantage of rectangular coordinates, its imaginary part does not exist. This may reduce the linearized equation (11) by one row and one column since the value of $\theta_0$ is known a priori, i.e., $\Delta\theta_0$ =0.

*c) Initial parameters and limits:*

Three VSC parameters require initialization. They are the amplitude modulation ratio ($m'_a$) and its phase angle ($\phi$). They are normally set at $\sqrt{3}/2$ and 0, respectively. The VSC is assumed to operate within the linear region, whereas the phase angle $\phi$ is assumed to have no limits. The third parameter is the equivalent shunt susceptance ($B_{eq}$), wich is given an initial value that lies within the range $B_{eq+}$ and $B_{eq-}$.

*E. VSC Test Cases*

The VSC model is applied in a rather contrived test case where the STATCOM is connected at the receiving end of a loaded transmission line to illustrate its performance, and for ease of reproduction. At this point in the paper, it is assumed that the STATCOM transformer is a conventional transformer and that its leakage reactance is lumped together with the reactance of the VSC. Hence, we shall refer to it as VSC as opposed to STATCOM. Three cases are considered: (i) the VSC is used to provide reactive power; (ii) the VSC is used to draw reactive power; and (iii) the VSC is used to supply a DC load.

*a) Test Case 1*

The three-node system shown in Fig. 2 comprises one generator, one transmission line and one AC/DC converter (VSC), which is represented by the elements shown within the broken-line rectangle.

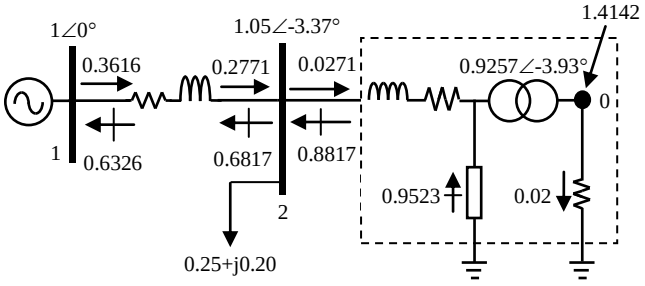


Figure 2: VSC providing voltage support at bus 2.

The generator node is taken to be the Slack bus where the voltage magnitude is kept at 1 p.u. and its phase angle provides a reference for all other phase angles in the network, excepting bus 0, where the phase angle is always zero in the STATCOM or VSC application. Bus 0 would be interpreted as the DC bus of the VSC circuit where the voltage is always a real quantity.

The following parameters are used in this system - (i) transmission line resistance and reactance: 0.05 p.u. and 0.10 p.u.; (ii) VSC series resistance and reactance: 0.01 p.u., 0.10 p.u.; (iii) VSC nominal values of shunt conductance and susceptance: 0.01 and 1.05 p.u.; (iv) active and reactive power load at node 2: 0.25 p.u. and 0.20 p.u.

As already stated in Section 4(b), the phase angle value at node 0 is independent of circuit parameters, network complexity and initializing conditions left of the phase shifter transformer - it is not specific to this circuit under test. To prove this point, different initial values are given to the Slack bus and the resulting voltages shown in Table I.

It should be noted that the phase angle voltage at bus 0 keeps its value given at the point of initialization and that in the application pursued in this paper, we shall stick to zero phase angle voltage initialization for this bus. When looked at it from the vantage of rectangular coordinates, its imaginary part does not exist. Indeed, an equivalent solution would be obtained by using a linearized equation akin to (11) but with no provision for the state variable $\theta_0$.

TABLE I
POWER FLOW SOLUTION FOR VARIOUS PHASE ANGLES AT THE SLACK BUS

| $V_1$ (p.u.) | $V_2$ (p.u.) | $V_0$ (p.u.) |
|---|---|---|
| 1∠0° | 1.05∠-3.37° | 1.4142∠0° → 1.4142 |
| 1∠-10° | 1.05∠-13.37° | 1.4142∠0° → 1.4142 |
| 1∠+10° | 1.05∠+6.63° | 1.4142∠0° → 1.4142 |

The phase angle difference between buses 1 and 2 is, in each case: -3.37°. The Newton-Raphson power flow algorithm converges in 7 iterations in all three cases, to a mismatch tolerance of $10^{-12}$. The symbol → is used in this table to signify "akin to".

The VSC consumes 0.0271 p.u. of active power from the system to account for its internal losses whilst supplying 0.8817 p.u. of reactive power to the system. The equivalent susceptance (in capacitive mode) produces 0.9523 p.u. of reactive power and its capacitive susceptance stands at $B_{eq}$=0.7408 p.u. As one would expect, the VSC switching losses are 2%, corresponding to a conductance $G_0$=1%. The DC bus voltage is controlled at 1.4142 p.u. and the voltage magnitude at bus 2 is kept at 1.05 with a 'true' $m_a$=0.9257. Notice that $m'_a$=0.8017. The phase shifter angle takes a value of -3.93°. The line current drawn by the VSC is 0.8402∠+84.87°.

For the sake of completeness, the test case is solved by modeling the VSC using its well-known representation based on the equivalent voltage source [1]-[4], which, in this case, has been extended to incorporate a shunt resistor to account for the VSC's switching losses.

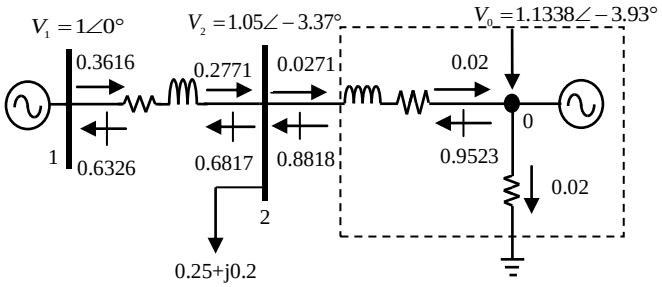


Figure 3: Test circuit using the conventional voltage source representation of the VSC.

Note that all the relevant parameters for this circuit are the same as in the circuit in Fig. 2, except that the resistance corresponding to the switching losses is connected on the left-hand side of the complex tap changer and, accordingly, it is affected by the square of the "off-nominal turns ratio" $m_a'$, i.e., $R_0$=0.01/0.8017$^2$. Node 0 is treated as a *PV*-type bus with zero active power injection and its voltage magnitude corresponds to the DC-like voltage of 1.4142 p.u. in the circuit of Fig. 2, affected by $m_a'$, i.e., $V_0$=1.4142×0.8017=1.1338.

The results were obtained using a conventional power flow program where bus 0 is treated as a PV bus with zero active power contribution and set to regulate voltage magnitude at the bus at 1.1338 p.u. As expected, the iterative solutions furnished by both modeling approaches yield similar results but the results at bus 0 merit additional analysis.The complex voltage at the equivalent voltage source corresponds to the cascading of the voltage at bus 0 in Fig. 2 and its phase shifter complex tap value. Furthermore, the reactive power contributed by the equivalent susceptance in the test circuit of Figure 2 equals the reactive power generated by the equivalent voltage source in the test circuit of Fig. 3.

The following limitations spring to mind in the voltage source model of the VSC compared to the new model introduced in this paper: (i) the voltage magnitude of the voltage source is difficult to determine since only the DC voltage is known and the amplitude modulation index ($m_a$) is not known a priori; (ii) by the same token, the switching losses will only be known approximately.

In this numerical example, the switching loss correction given by eq. (3) was not applied in order to be able to

compare the response furnished by the two VSC models, namely, the new VSC model and the equivalent voltage source model. In any case, little change is expected since the current magnitude (0.8402 p.u.) is close to the 1 p.u. rated current. Perhaps the most noticeable change is a reduction in the switching loss from 2% to 1.4% and the ensuing adjustment in active power flows.

*b) Test Case 2*

The operating conditions of the power circuit in Test Case 1 are modified to force the VSC to draw reactive power from the slack generator connected at bus 1.

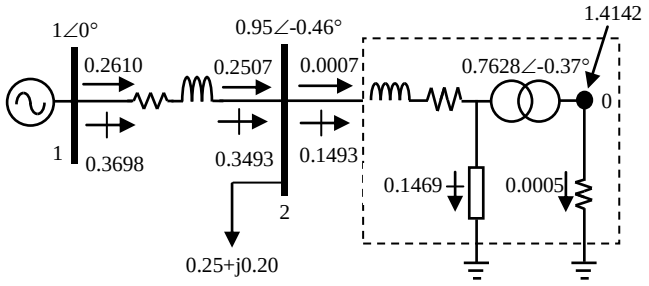


Figure 4: The test network uses the same circuit parameters as in Test Case 1 but the voltage magnitude at bus 2 is kept at 0.95 p.u. using $m_a$ to force the reactive power flow into the VSC.

The VSC draws 0.0007 p.u. of active power and 0.1493 p.u. of reactive power. The equivalent susceptance absorbs 0.1469 p.u. of reactive power and its inductive susceptance stands at $B_{eq}$=-0.1682 p.u. The VSC switching losses are low, 0.05%, since the current drawn by the VSC is quite small, i.e. 0.1572∠-90.17° p.u. The DC bus voltage is controlled at 1.4142 p.u. and the voltage magnitude at bus 2 is kept at 0.95 with $m_a$=0.7628. The phase shifter angle takes a value of -0.37°.

*c) Test Case 3*

Test Case 1 is expanded to incorporate a load in the DC side of the VSC in the form of a battery system which is assumed to take a constant power of 0.5 p.u.

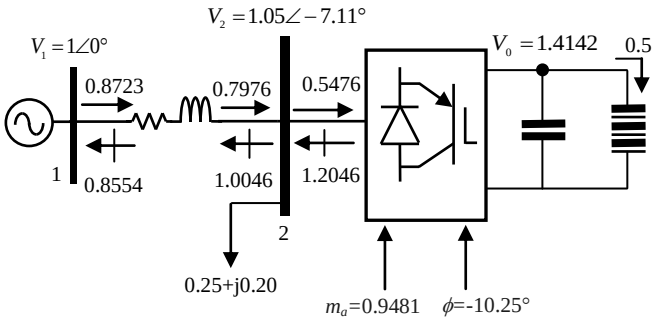


Figure 5: Test network with a battery load on its DC bus

This test network uses the same circuit parameters as in Test Case 1 but a second load is added in the form of a battery which is being supplied through the VSC at 0.5 p.u. of power. The VSC is used to keep the voltage magnitude at 1.05 p.u. at bus 2.

The total VSC active power loss stands at 4.76% p.u. where 3.18% corresponds to switching loss and 1.58% corresponds to ohmic loss. The VSC contributes 1.2046 p.u. to supply the reactive power load of 0.20 p.u. and the rest being exported to the Slack generator. The VSC equivalent susceptance with a capacitive value of $B_{eq}$=1.0111 p.u. produces 1.3634 p.u. of reactive power. The SVC is set to regulate voltage magnitude at its AC bus at 1.05 p.u. and its actual complex modulation ratio is: 0.9481∠-10.25°. The current drawn by the VSC is 1.2602∠+58.44°. The solution converges in 7 iterations to a tolerance of $10^{-12}$.

## III. Power Flow STATCOM Model

For studies at the fundamental frequency, the STATCOM may be seen to comprise a VSC and an interfacing transformer, which may be a load tap changer (LTC). The VSC schematic representation and equivalent circuit are given in Fig. 1 and the equivalent circuit of the LTC transformer is given in Fig. 6.

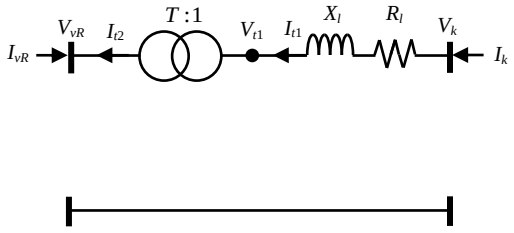


Figure 6: LTC transformer equivalent

Inclusion of the STATCOM model in a power flow solution is straightforward. It only requires explicit representation of the nodal power flow equations of the VSC connected between say, nodes 0 and *VR*, and the nodal power equations of the LTC transformer connected between say, nodes *VR* and *K*. Alternatively, a more compact set of power flow equations may be achieved by realizing that the interface point between the VSC and LTC circuits, namely *vR* node, receives a zero external (nodal) current injection. Then a mathematical elimination of node *vR* becomes an option. However, it should be noted that this reduced model is only attractive if we are prepared to lose a degree of modeling flexibility, since this bus is not explicitly available for regulating action of either $T$ or $m_a'$. Instead, the combined regulating action will take place in the high-voltage side of the LTC transformer.

### *A. Reduced STATCOM nodal admittance matrix*

The nodal admittance matrix of the LTC transformer in Fig. 6, is:

$$\begin{pmatrix} \bar{I}_k \\ \bar{I}_{vR} \end{pmatrix} = \begin{pmatrix} \bar{Y}_l & -T\bar{Y}_l \\ -T\bar{Y}_l & T^2\bar{Y}_l \end{pmatrix} \begin{pmatrix} \bar{V}_k \\ \bar{V}_{vR} \end{pmatrix} \tag{15}$$

Combining the two individual models yields the compound model representing the VSC-LTC or STATCOM model:

$$\begin{pmatrix} \bar{I}_k \\ \bar{I}_{vR} \\ \bar{I}_0 = 0 \end{pmatrix} = \begin{pmatrix} \bar{Y}_l & -T\bar{Y}_l & 0 \\ -T\bar{Y}_l & T^2\bar{Y}_l + \bar{Y}_1 & -m'_a \angle\phi\, \bar{Y}_1 \\ 0 & -m'_a \angle -\phi\, \bar{Y}_1 & G_{sw} + m'^2_a(\bar{Y}_1 + \mathrm{j}B_{eq}) \end{pmatrix} \begin{pmatrix} \bar{V}_k \\ \bar{V}_{vR} \\ V_0 = E_{DC} \end{pmatrix} \tag{16}$$

Mathematical elimination of node *vR* yields the following reduced nodal admittance matrix:

$$\begin{pmatrix} \bar{I}_k \\ \bar{I}_0 = 0 \end{pmatrix} = \frac{1}{\Delta} \begin{pmatrix} \bar{Y}_1 \bar{Y}_l & -Tm'_a \angle\phi \bar{Y}_l \bar{Y}_1 \\ -Tm'_a \angle -\phi \bar{Y}_l \bar{Y}_1 & T^2 m'^2_a \bar{Y}_l \bar{Y}_1 + (T^2 \bar{Y}_l + \bar{Y}_1)\bar{Y}_{eq} \end{pmatrix} \begin{pmatrix} \bar{V}_k \\ V_0 = E_{DC} \end{pmatrix} \tag{17}$$

where $\Delta = T^2 \bar{Y}_l + \bar{Y}_1$ and $\bar{Y}_{eq} = G_{sw} + jm'^2_a B_{eq}$.

*B. STATCOM nodal power equations*

Following a similar procedure as in section II-*C* for the derivation of the nodal power equations of the VSC, the active and reactive power expressions for the STATCOM model are derived:

$$\begin{aligned}
P_k &= G_{eq\,l1} V_k^2 - Tm'_a V_k V_0 \left[ G_{eq\,l1} \cos(\theta_k - \theta_0 - \phi) + B_{eq\,l1} \sin(\theta_k - \theta_0 - \phi) \right] \\
Q_k &= -B_{eq\,l1} V_k^2 - Tm'_a V_k V_0 \left[ G_{eq\,l1} \sin(\theta_k - \theta_0 - \phi) - B_{eq\,l1} \cos(\theta_k - \theta_0 - \phi) \right] \\
P_0 &= \left( T^2 m'^2_a G_{eq\,l1} + T^2 G_{eq\,l0} + G_{eq\,10} \right) V_0^2 - Tm'_a V_k V_0 \left[ G_{eq\,l1} \cos(\theta_0 - \theta_k + \phi) \right. \\
&\qquad \left. + B_{eq\,l1} \sin(\theta_0 - \theta_k + \phi) \right] \\
Q_0 &= -\left( T^2 m'^2_a B_{eq\,l1} + T^2 B_{eq\,l0} + B_{eq\,10} \right) V_0^2 - Tm'_a V_k V_0 \left[ G_{eq\,l1} \sin(\theta_0 - \theta_k + \phi) \right. \\
&\qquad \left. - B_{eq\,l1} \cos(\theta_0 - \theta_k + \phi) \right]
\end{aligned} \tag{18}$$

where

$$G_{eq\,l1} = \frac{1}{\Delta}\left[ T^2 G_1 \left( G_l^2 + B_l^2 \right) + G_l \left( G_1^2 + B_1^2 \right) \right]$$

$$B_{eq\,l1} = \frac{1}{\Delta}\left[ T^2 B_1 \left( G_l^2 + B_l^2 \right) + B_l \left( G_1^2 + B_1^2 \right) \right]$$

$$G_{eq\,10} = \frac{1}{\Delta}\left[ T^2 B_l \left( m'^2_a G_1 B_{eq} + B_1 G_{sw} \right) + T^2 G_l \left( G_1 G_{sw} - m'^2_a B_1 B_{eq} \right) + G_{sw} \left( G_1^2 + B_1^2 \right) \right]$$

$$B_{eq\,10} = \frac{1}{\Delta}\left[ T^2 G_l \left( m'^2_a G_1 B_{eq} + B_1 G_{sw} \right) - T^2 B_l \left( G_1 G_{sw} - m'^2_a B_1 B_{eq} \right) + m'^2_a B_{eq} \left( G_1^2 + B_1^2 \right) \right]$$

$$G_{eq\,l0} = \frac{1}{\Delta}\left[ T^2 G_{sw0} \left( G_l^2 + B_l^2 \right) + B_l \left( B_1 G_{sw} - m'^2_a G_1 B_{eq} \right) + G_l \left( G_1 G_{sw} + m'^2_a B_1 B_{eq} \right) \right]$$

$$B_{eq\,l0} = \frac{1}{\Delta}\left[ T^2 m'^2_a B_{eq} \left( G_l^2 + B_l^2 \right) - G_l \left( B_1 G_{sw} - m'^2_a G_1 B_{eq} \right) + B_l \left( G_1 G_{sw} + m'^2_a B_1 B_{eq} \right) \right]$$

$$\Delta = \left( T^2 G_l + G_1 \right)^2 + \left( T^2 B_l + B_1 \right)^2$$

The numerical solution of equation system (18), for a pre-defined set of generation and load pattern, is carried out very efficiently by iteration using the Newton-Raphson method. Similarly to the VSC model in Section II-*C*, this involves repeated linearization of the nodal power equations and their initial evaluation requires an informed guess of the state variables values: $(\theta_k^{(0)}, \theta_0^{(0)}, T, m'^{(0)}_a, \phi^{(0)}, B_0^{(0)})$. The linearized system of equations may be compacted further by eliminating the row and column associated to the variable $\theta_0$, since this is a priori known variable that keeps its value at the point of initialization, which in this application is zero. The ensuing equation is:

$$\begin{bmatrix} \Delta P_k \\ \Delta Q_k \\ \hline \Delta P_{0\text{-}k} \\ \Delta Q_{0\text{-}k} \end{bmatrix}^{(r)} = \begin{bmatrix} \partial P_k/\partial\theta_k & (\partial P_k/\partial Tm'_a)Tm'_a & \partial P_k/\partial\phi & \partial P_k/\partial B_0 \\ \partial Q_k/\partial\theta_k & (\partial Q_k/\partial Tm'_a)Tm'_a & \partial Q_k/\partial\phi & \partial Q_k/\partial B_0 \\ \hline \partial P_{0\text{-}k}/\partial\theta_k & (\partial P_{0\text{-}k}/\partial Tm'_a)Tm'_a & \partial P_{0\text{-}k}/\partial\phi & \partial P_{0\text{-}k}/\partial B_0 \\ \partial Q_{0\text{-}k}/\partial\theta_k & (\partial Q_{0\text{-}k}/\partial Tm'_a)Tm'_a & \partial Q_{0\text{-}k}/\partial\phi & \partial Q_{0\text{-}k}/\partial B_0 \end{bmatrix}^{(r)} \begin{bmatrix} \Delta\theta_k \\ \Delta Tm'_a/Tm'_a \\ \hline \Delta\phi \\ \Delta B_0 \end{bmatrix}^{(r)} \tag{19}$$

where $Tm_a'$ is used to signify the use of either $T$ or $m_a'$.

The attraction of (19) is its rather compact nature in representing the combined operation of the VSC and the LTC transformer with only four variables. However, this comes at a price – some modeling flexibility is lost. Notice that since the connecting bus between the VSC and the LTC is not explicitly available in this combined model, it cannot be controlled by the regulating action of either $T$ or $m_a'$. Also, since the DC bus is regulated by the action of the DC capacitor and treated in the power flow solution as a *PV* bus then $T$ and $m_a'$ are available solely for the purpose of regulating voltage magnitude at the high-voltage bus of the LTC transformer. Hence, the regulating action of $T$ and $m_a'$ is sequential in this model. It should be emphasized that, from the power flow solution vantage, there is no actual restriction in attempting to control the DC bus voltage with either $T$ or $m_a'$. However, from the equipment operation point of view, this regulating action is hardly ever done.

Subsequent evaluations of the nodal power equations are carried out using the improved set of values furnished by the iterative process: $(\theta_k^{(r)}, \theta_0^{(r)}, T^{(r)}, m'^{(r)}_a, \phi^{(r)}, B_0^{(r)})$, where $(r)$ is the iteration counter. It should be noticed that in this formulation, the control capabilities have been extended compared to that of the VSC in (11). It becomes possible to regulate nodal voltage magnitude at the STATCOM terminal (bus *k*) using the combined action of the LTC tap ($T$) and the VSC amplitude modulation coefficient ($m_a'$), one at the time. It should be remarked that in an actual VSC, $m_a'$ takes continuous values and that in an actual LTC transformer, the tap $T$ takes discrete values. Nevertheless, for the purpose of the power flow model using the Newton-Raphson method and aiming at maintaining the quadratic convergence characteristic of this iterative algorithm, the variable $T$ is assumed to take continuous values. It is at the end of the iterative solution that the tap $T$ is moved to the nearest physical tap value and then nodal voltages are re-adjusted and power flows and power losses calculated.

The mismatch power terms and control variables remain the same as in (12), except that the subscript *k* replaces the subscript *vR*. In the state variables increments in (13) the subscript *vR* is also replaced by the subscript *k* and the newly introduced state variable $Tm_a'$ replaces $m_a'$,

$$\begin{aligned} \Delta\theta_k^{(r)} &= \theta_k^{(r)} - \theta_k^{(r-1)} \\ \Delta Tm'^{(r)}_a &= Tm'^{(r)}_a - Tm'^{(r-1)}_a \end{aligned} \tag{20}$$

where $T$ and $m_a'$ are normally initialized at 1 and $\sqrt{3}/2$, respectively.

*C. STATCOM Test Cases*

Two test cases are presented in this section to illustrate the control flexibility afforded by the reduced STATCOM model. The first case relates to a contrived system which is, essentially, the same system as that used in Test Case 1, except that the STACOM model replaces the VSC model. The second test case is a modified version of the IEEE 30-node system [16] where two STATCOMs regulate voltage magnitude at two different points in the network.

*a) Test Case 4*

The power circuit in Test Case 1 is modified to replace the VSC connected at bus 2 by a STATCOM, where the LTC's STATCOM figures prominently in Fig. 7.

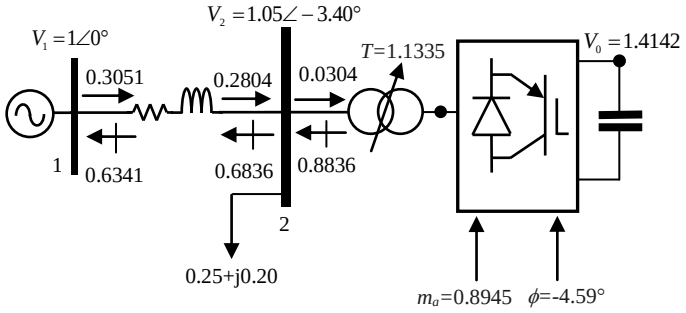


Figure 7: Upgraded network used in Test Case 1, to include the LTC transformer

The test network uses the same circuit parameters as in Test Case 1 except that the parameters of the LTC transformer are added to the circuit parameters: $R_T$=0.01 p.u. and $X_T$=0.10 p.u. The tap limits are: $0.8<T<1.2$. The generator keeps the voltage magnitude at the slack node at 1 p.u. The STATCOM consumes 0.0304 p.u. of active power from the system to account for its internal losses whilst supplying 0.8836 p.u. of reactive power to the system. The VSC switching losses stand at $G_0$=1.42% and the remaining 1.62% correspond to ohmic losses in the LTC transformer and VSC. The DC bus voltage is kept at 1.4142 p.u. by action of the DC capacitor and this bus is treated in the power flow solution as a *PV* bus. The voltage magnitude at bus 2 is kept at 1.05 p.u. with a combination of a selected $m_a$ of 0.8945 and a resulting transformer tap of $T$=1.1335. The current drawn by the STATCOM is $0.8421\angle+84.63°$.

*b) Test Case 5*

In order to test the performance of the proposed STATCOM model in a larger power network, the IEEE 30-node system is selected [16]. The fix banks of capacitors at nodes 10 and 24 in the original network are replaced with STATCOMs which are set to regulate voltage magnitudes at their points of connection with the power grid. Their respective DC voltages are kept at 1.4142 p.u. The relevant portions of the modified 30-bus system are shown in Fig. 8.

The voltage magnitudes at the compensated buses, namely, 10 and 24, are compared in Table II to the case when conventional capacitor banks are connected to these nodes, and when no compensation is used.

TABLE II
VOLTAGE MAGNITUDES AT THE COMPENSATED BUSES IN THE 30-BUS SYSTEM FOR TWO COMPENSATION OPTIONS

| Compensation Case | VOLTAGE MAGNITUDE (P.U.) | |
|---|---|---|
| | Bus 10 | Bus 24 |
| *None* | 0.9703 | 0.9480 |
| *Fix* | 0.9957 | 0.9731 |
| *STATCOMs* | 0.9957 | 0.9731 |

The two STATCOMs use identical parameters and their LTC transformers are set at their nominal tap positions ($T$=1). They are assumed to contain no resistance and their reactances are $X_{TR}$=0.05 p.u. The VSCs series and shunt parameters, in per-unit, are: $R_1$=0.01, $X_1$=0.05, $G_{sw}$=0.01 and $B_{eq}$=0.50, respectively.

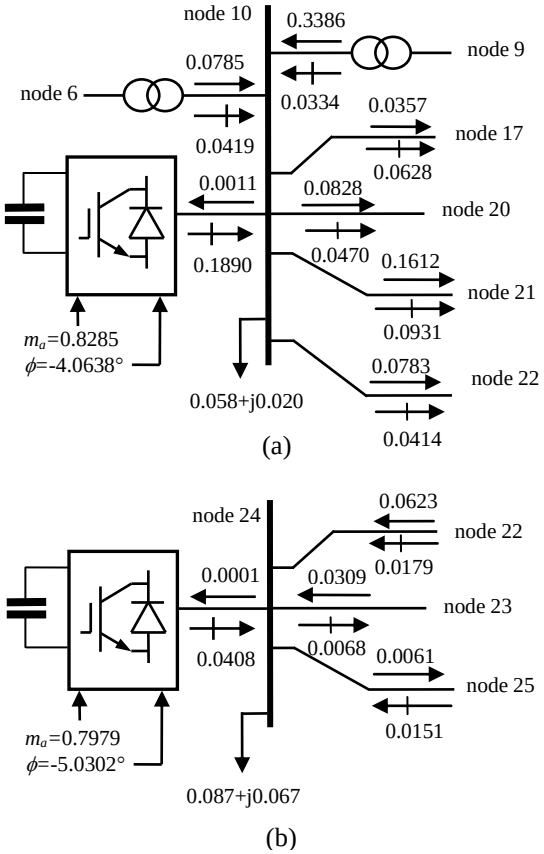


Figure 8: STATCOMs supplying reactive power at buses 10 and 24 of the modified IEEE 30-bus system

The susceptance values used for the case with fix compensation at buses 10 and 24 are 0.19 p.u. and 0.043 p.u., which are the values given in [16]. For the STATCOM case, the voltages at buses 10 and 24 are kept at the same level as those given by the case with fix compensation. As expected, one benefit of shunt compensation is to reduce the system power losses due to an improved voltage profile, and this trend is shown in the power loss figures presented in Table III. The STATCOM-type compensation introduces an additional kind of power loss which is associated with the high-frequency switching of the PWM control used by the VSC technology and ohmic losses. The STATCOM losses are quite low in this case because the currents drawn by the two STATCOMs are low compared to the 1 p.u. rated currents namely, $0.1899\angle+85.73°$ p.u. and $0.0419\angle+84.92°$ p.u.

TABLE III
POWER LOSS AT THE COMPENSATED BUSES IN THE 30-BUS SYSTEM FOR TWO COMPENSATION OPTIONS

| Compensation Case | ACTIVE POWER LOSS (%) | |
|---|---|---|
| | Network | STATCOMs |
| *None* | 3.12 | - |
| *Fix* | 2.89 | - |
| *STATCOMs* | 2.94 | 0.12 |

The power flow solutions converged in 6 iterations for the first two cases and in 7 iterations for the STATCOMs, to mismatch a tolerance of $10^{-12}$.

## IV. CONCLUSIONS

A new STATCOM model aimed at power flow solutions using the Newton-Raphson method has been introduced. The model represents a paradigm shift in the way the fundamental frequency, positive sequence VSC-FACTS controllers are represented. It does not treat the controller as an idealized controllable voltage source but rather as a compound transformer device to which certain control properties of PWM-based inverters may be linked. This argument is similar to the one advanced for DC-to-DC converters which have been linked, conceptually speaking, to step-up and step-down transformers [19]. The phase angle of the complex tap changer represents the phase shift that would exist in a PWM inverter and coincides with the phase angle of the conventional voltage source model of the VSC. More specifically, this would be the phase angle required by the VSC to enable either reactive power generation or absorption purely by electronic processing of the voltage and current waveforms within the VSC. The switching losses, ohmic losses and the connecting LTC transformer are all explicitly represented in the new STATCOM model. The complex tap changer in the VSC model and the real tap changer in the LTC model enable an effective voltage regulation at the point of connection with the grid and at the VSC's AC node. The model has been tested in a simple system for ease of reproduction by interested parties. A larger power system has also been used to show that the new STATCOM power flow model retains its strong convergence characteristics.

## ACKNOWLEDGEMENTS

The authors wish to acknowledge the most valuable and insightful criticisms made by the referees of this paper, which have enhanced the theoretical basis on which this STATCOM model has been developed.

## REFERENCES

[1] G.N. Hingorani and L. Gyugyi, *Understanding FACTS: concepts and technologies of flexible ac transmission systems.* IEEE 2000.

[2] E. Acha, C.R. Fuerte-Esquivel, H. Ambriz-Perez and C. Angeles-Camacho, *FACTS modeling and simulation in power networks.* John Wiley & Sons, 2005.

[3] D. J. Gotham and G. T. Heydt, "Power flow control and power flow studies for systems with FACTS devices", *IEEE Trans. Power Systems*, vol. 13, pp. 60-65, Feb. 1998

[4] X. Zhang and E. J. Handschin, "Optimal power flow control by converter based FACTS controllers", presented at Seventh Int. Conf. on AC-DC Power Transmission, (Conf. Publ. No. 485), pp. 250-255, 28-30 Nov. 2001

[5] D.M. Brod and D.M. Novotny, "Current Control of VSI-PWM Inverters", IEEE Trans. on Industry Applications, vol. 21, no. 4, pp. 562-570, 1985.

[6] H.W. van der Broeck, H.C. Skudelny and G.V. Stanke, "Analysis and Realisation of Pulsewidth Modulator based on Voltage Space Vectors", IEEE Trans. on Industry Applications, vol. 24, no. 1, pp. 142-150, 1988.

[7] R. Wu, S.B. Dewan and G.R. Slemon, "A PWM AC-to-DC Converter with Fixed Switching Frequency", IEEE Trans. on Industry Applications, vol. 26, no. 5, pp. 880-885, 1990.

[8] R. Wu, S.B. Dewan and G.R. Slemon, "Analysis of an PWM AC-to-DC Voltage Source Converter Using PWM with Phase and Amplitude Control", IEEE Trans. on Industry Applications, vol. 27, no. 2, pp. 355-364, 1991.

[9] C.A. Cañizares, "Power Flow and Transient Stability Models of FACTS Controllers for Voltage and Angle Stability Studies", IEEE PES WM, 23-27 Jan. 2000, Singapore, pp. 1447-1454,2000.

[10] C. Angeles-Camacho, O. L. Tortelli, E. Acha and C. R. Fuerte-Esquivel, "Inclusion of a high voltage dc-voltage source converter model in a Newton-Raphson power flow algorithm", in *IEE Proc. Gen., Trans. and Dist.*, vol. 150, pp. 691-696, Nov. 2003

[11] L. Gyugyi, "Dynamic Compensation of AC Transmission Lines by Solid-State Synchronous Voltage Sources", IEEE Trans. on Power Delivery, vol. 9, no. 2, pp. 904-911, April 1994.

[12] S. An and T.W. Gedra, "UPFC Ideal Transformer Model", Proc. North American Power Symposium (NAPS), pp. 46-50, Oct. 2003.

[13] S. An, J. Condren and T.W. Gedra, "An Ideal Transformer Model, OPF First-Order Sensitivities, and Application to Screening for Optimal UPFC Locations", IEEE Trans. on Power Systems, vol. 22, no. 1, pp. 68-75, Feb. 2007.

[14] C.R. Fuerte-Esquivel, E Acha and H. Ambriz-Perez, "A Comprehensive Newton-Raphson UPFC Model for the Quadratic Power Flow Solution of Practical Power Networks", IEEE Trans. on Power Systems, vol. 15, no. 1, pp. 102-109, Feb. 2000.

[15] H. Ambriz-Perez, E Acha, C.R. Fuerte-Esquivel, and A. de la Torre, "Incorporation of a UPFC Model in an Optimal Power Flow Using Newton's method", IEE Proc. Gen., Trans. and Dist., vol. 145, no. 3, pp. 336-344, May 1998.

[16] IEEE 30-node Test System. Available: http://www.ee.washington.edu/research/pstca

[17] C.J.M. Verhoeven, A. van Staveren, G.L.E. Monna, M.H.L. Kouwenhoven and E. Yildiz, *Structured Electronic Design: Negative Feedback Amplifiers.* Kluwer Academic, 2003.

[18] J.W. Nilsson and S. Riedel, *Electric Circuits* (9th Edition). Prentice Hall, 2010.

[19] N. Mohan, T.M. Undeland and W.P. Robins, *Power Electronics: Converters, Applications and Design.* John Wiley & Sons, 2003.

## APPENDIX A: THE IDEAL PHASE SHIFTER CIRCUIT

One salient characteristic of the new VSC model is that no special provisions within a conventional AC power flow solution algorithm is required to represent the DC circuit, since the complex tap-changing transformer of the VSC may be used with ease to give rise to the customary AC circuit and a notional DC circuit. However, some further explanation is required since the modelling development involves the conflation of AC and DC circuit concepts at an equivalent node, brought about by the use of the ideal tap-changing transformer concept.

In order to elaborate the explanation from the vantage of electronic circuits, we are going to assume that the conductance associated with switching losses, $G_{sw}$, in Fig. 1(b), may be referred to the primary side of the ideal transformer. The relevant part of the circuit illustrating such a situation but with capacitor representation, as opposed to its equivalent battery representation, is shown in Fig. A.1,

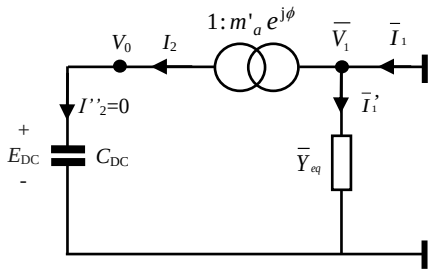


Figure A.1: Equivalent circuit showing the ideal phase-shifting transformer of Fig. 1(b) and neighboring elements, where $\bar{Y}_{eq} = G_{sw} + jB_{eq}$.

By invoking eq. (4),

$$I_2 = m'_a\, e^{-j\phi}(\bar{I}_1 - \bar{I}'_1) = I''_2 = 0 \quad \text{(A.1)}$$

$$V_0 = \frac{\bar{V}_1}{m'_a\, e^{j\phi}} = \frac{V_1 e^{j\phi}}{m'_a\, e^{j\phi}} = \frac{V_1}{m'_a} = E_{\mathrm{DC}} \quad \text{(A.2)}$$

In steady-state, a charged DC capacitor draws zero current and it is well-accepted that it may be represented as a charged battery [18] and, by extension, as a DC voltage source feeding no current. These facts are reflected by (A.1) and (A.2) and give the opportunity to interpret the circuit in Fig. A.1 in terms of electronic circuits concepts. Hence, it may be argued that in steady-state this circuit behaves as a *nullor* operating on a DC source representing the DC capacitor. The *nullor* is made up of a *nullator* and a *norator* [17], represented in this case by the ideal phase-shifting transformer and the equivalent admittance, $\bar{Y}_{eq}$, respectively. The circuit in Fig. A.1 may be re-drawn as follows,

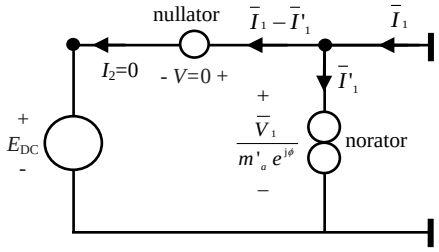


Figure A.2: Interpretation of the equivalent circuit of Fig. A.1 in terms of electronic circuit elements

The nullator and the norator are said to be linear, time-invariant one-port elements. The former is defined as having zero current through it and zero voltage across it. The latter, on the other hand, can have an arbitrary current through it and an arbitrary voltage across its terminals. Nullators have properties of both short-circuit (zero voltage) and open-circuit (zero current) connections. They are current and voltage sources at the same time. A norator is a voltage or current source with infinite gain. It takes whatever current and voltage is required by the external circuit to meet Kirchhoff's circuit laws. A norator is always paired with a nulator [17].

Either, by careful examination of (A.1) and (A.2) or by analysis of the electronic equivalent circuit in Fig. A.2, it can be seen that the ideal, complex tap-changing transformer of the VSC gives raise to the customary AC circuit and a notional DC circuit where the DC capacitor yields voltage $E_{\mathrm{DC}}$ but draws no current.

In a more general sense and from the viewpoint of the AC power flow solution, if resistive elements or DC power loads are connected to the notional DC bus then currents do pass through the ideal phase-shifting transformer but it would be a component of current that yields a nodal voltage $V_0$ with zero phase angle and, as one would expect, yields power with no imaginary component, hence, no reactive power exists in this part of the notional DC circuit.

## APPENDIX B: PARTIAL DERIVATIVE TERMS FOR THE VSC

The partial derivative terms making up the Jacobian matrix in eqn. (11) are given below. Note that these derivative terms do not include the current dependency in the switching loss term $G_{SW}$ – refer to (3).

$$\partial P_{vR}/\partial\theta_{vR} = -Q_{vR,\mathrm{cal}} - B_1 V_{vR}^2 \quad \text{(B.1)}$$

$$\partial Q_{vR}/\partial\theta_{vR} = P_{vR,\mathrm{cal}} - G_1 V_{vR}^2 \quad \text{(B.2)}$$

$$(\partial P_{vR}/\partial m'_a)m'_a = P_{vR,\mathrm{cal}} - G_1 V_{vR}^2 \quad \text{(B.3)}$$

$$(\partial Q_{vR}/\partial m'_a)m'_a = Q_{vR,\mathrm{cal}} + B_1 V_{vR}^2 \quad \text{(B.4)}$$

$$\partial P_{vR}/\partial\theta_0 = Q_{vR,\mathrm{cal}} + B_1 V_{vR}^2 \quad \text{(B.5)}$$

$$\partial Q_{vR}/\partial\theta_0 = -P_{vR,\mathrm{cal}} + G_1 V_{vR}^2 \quad \text{(B.6)}$$

$$\partial P_0/\partial\theta_{vR} = Q_{0,\mathrm{cal}} + m'^2_a(B_{eq} + B_1)V_0^2 \quad \text{(B.7)}$$

$$(\partial P_0/\partial m'_a)m'_a = P_{0,\mathrm{cal}} - (G_0 - m'^2_a G_1)V_0^2 \quad \text{(B.8)}$$

$$\partial P_0/\partial\theta_0 = -Q_{0,\mathrm{cal}} - m'^2_a(B_{eq} + B_1)V_0^2 \quad \text{(B.9)}$$

$$\partial P_{vR}/\partial\phi = Q_{vR,\mathrm{cal}} + B_1 V_{vR}^2 \quad \text{(B.10)}$$

$$\partial Q_{vR}/\partial\phi = -P_{vR,\mathrm{cal}} + G_1 V_{vR}^2 \quad \text{(A.11)}$$

$$\partial P_{vR}/\partial B_0 = 0 \quad \text{(B.12)}$$

$$\partial Q_{vR}/\partial B_0 = 0 \quad \text{(B.13)}$$

$$\partial P_0/\partial\phi = -Q_{0,\mathrm{cal}} - m'^2_a(B_{eq} + B_1)V_0^2 \quad \text{(B.14)}$$

$$\partial P_0/\partial B_0 = 0 \quad \text{(B.15)}$$

$$\partial P_{0-vR}/\partial\theta_{vR} = \partial P_0/\partial\theta_{vR} \quad \text{(B.16)}$$

$$(\partial P_{0-vR}/\partial m'_a)m'_a = (\partial P_0/\partial m'_a)m'_a \quad \text{(B.17)}$$

$$\partial P_{0-vR}/\partial\theta_0 = \partial P_0/\partial\theta_0 \quad \text{(B.18)}$$

$$\partial P_{0-vR}/\partial\phi = \partial P_0/\partial\phi \quad \text{(B.19)}$$

$$\partial P_{0-vR}/\partial B_0 = \partial P_0/\partial B_0 \quad \text{(B.20)}$$

$$\partial Q_{0-vR}/\partial\theta_{vR} = \partial Q_0/\partial\theta_{vR} = -P_{0,\mathrm{cal}} + (G_0 + m'^2_a G_1)V_0^2 \quad \text{(B.21)}$$

$$(\partial Q_{0-vR}/\partial m'_a)m'_a = (\partial Q_0/\partial m'_a)m'_a = Q_{0,\mathrm{cal}} - m'^2_a(B_{eq} - B_1)V_0^2 \quad \text{(B.22)}$$

$$\partial Q_{0-vR}/\partial\theta_0 = \partial Q_0/\partial\theta_0 = P_{0,\mathrm{cal}} - (G_0 + m'^2_a G_1)V_0^2 \quad \text{(B.23)}$$

$$\partial Q_{0-vR}/\partial\phi = \partial Q_0/\partial\phi = P_{0,\mathrm{cal}} - (G_0 + m'^2_a G_1)V_0^2 \quad \text{(B.24)}$$

$$\partial Q_{0-vR}/\partial B_0 = \partial Q_0/\partial B_0 = -m'^2_a V_0^2 \quad \text{(B.25)}$$

**Enrique Acha** (SM'02) was born in Mexico. He graduated from Universidad Michoacana in 1979 and obtained his PhD degree from the University of Canterbury, Christchurch, New Zealand, in 1988. He was the Professor of Electrical Power Systems at the University of Glasgow, UK in the period 2001-2011 and he is now the Professor of Electrical Power Systems at the Tampere University of Technology (TUT), Finland. He is an IEEE PES distinguished lecturer.

**Behzad Kazemtabrizi** was born in Tehran, Iran. He received his BSc in Electrical Power Engineering from Azad University, Tehran Iran in 2006. He then received his MSc and PhD degrees in Electronics and Electrical Engineering from the University of Glasgow, Scotland, UK in 2007 and 2011, respectively. He is now with the School of Engineering and Computer Science in Durham University working as a Research Associate. He has been a student member of IEEE since 20007.